Earth Syst. Dynam. Discuss., 6, 81–132, 2015
www.earth-syst-dynam-discuss.net/6/81/2015/
doi:10.5194/esdd-6-81-2015

Earth System Dynamics Discussions
Open Access

Propagation of biases in humidity in the estimation of global irrigational water

Y. Masaki, N. Hanasaki, K. Takahashi, and Y. Hijioka

National Institute for Environmental Studies, 16-2 Onogawa,
Tsukuba, Ibaraki, 305-8506, Japan

Received: 25 December 2014 – Accepted: 8 January 2015 – Published: 26 January 2015

Correspondence to: Y. Masaki (masaki.yoshimitsu@nies.go.jp)

Published by Copernicus Publications on behalf of the European Geosciences Union.

Abstract

Future projections on irrigational water under a changing climate are highly dependent on meteorological data derived from general circulation models (GCMs). Since climate projections include biases, bias correction is widely used to adjust meteorological elements, such as the atmospheric temperature and precipitation, but less attention has been paid to biases in humidity. Hence, in many cases, raw GCM outputs have been directly used to analyze the impact of future climate change. In this study, we examined how the biases remaining in the humidity data of five GCMs propagate into the estimation of irrigational water demand and abstraction from rivers using the global hydrological model (GHM) H08. First, to determine the effects of humidity bias across GCMs, we used meteorological data sets to which a state-of-the-art bias correction method was applied except to the humidity. Uncorrected GCM outputs were used for the humidity. We found that differences in the monthly relative humidity of 11.7 to 20.4 % RH (percent used as the unit of relative humidity) from observations across the GCMs caused the estimated irrigational water abstraction from rivers to range between 1217.7 and 1341.3 $km^3\,yr^{-1}$ for 1971–2000. Differences in humidity also propagate into future projections. Second, sensitivity analysis with hypothetical humidity biases of ±5 % RH added homogeneously worldwide revealed the large negative sensitivity of irrigational water abstraction in India and East China, which have high areal fractions of irrigated cropland. Third, we performed another set of simulations with bias-corrected humidity data to examine whether bias correction of the humidity can reduce uncertainties in irrigational water across the GCMs. The results showed that bias correction, even with a primitive methodology that only adjusts the monthly climatological relative humidity, helped reduce uncertainties across the GCMs. Although the GHMs have different sensitivities to atmospheric humidity because of the implementation of different types of potential evapotranspiration formulae, bias correction of the humidity should be included in hydrological analysis, particularly for the evaluation of evapotranspiration and irrigational water.

ESDD
6, 81–132, 2015

1 Introduction

Recent ongoing global warming is expected to change current hydroclimatological environments at the global scale. Since fresh water is essential for various industrial and social activities of human beings, its availability plays a crucial role in the sustainable development of society.

Agriculture is one of the human activities that are highly susceptible to hydroclimatological conditions. Irrigated water applied to cropland is primarily lost through evapotranspiration. According to Vörösmarty et al. (2005) (Tables 7.3 and 7.4), the total amount of global freshwater withdrawal was 3560 $km^3 yr^{-1}$ for 1995–2000, 2480 $km^3 yr^{-1}$ (70 % of the total withdrawal) was supplied for agricultural use, and the consumptive loss through evapotranspiration from irrigated cropland amounted to 1210 $km^3 yr^{-1}$ (34 % of the total human withdrawal and 49 % of the total agricultural withdrawal). In Asia, a larger portion of abstracted water is lost through evapotranspiration (52 % of the total human withdrawal and 59 % of the total agricultural withdrawal) than the global average. Therefore, the evapotranspiration loss from irrigated cropland plays a crucial role in the amount of irrigational water abstraction. Moreover, the volume of irrigation water is expected to increase in the future because of an increase in evapotranspiration from cropland under warmer climates and the expansion of irrigated cropland to meet the increasing demand for food owing to the increase in the world population. Precise estimation of the amount of irrigational water abstraction is crucial for the sustainable use of available water in the future.

To quantitatively evaluate future irrigational water, we must substantially rely on hydrological simulation. However, there are fundamental difficulties in the estimation because there are many possible errors and uncertainties in the data sets (meteorological data sets, land use data, etc.), calculation schemes (evapotranspiration, runoff, river flow, etc.) and parameters. In fact, different general circulation models (GCMs) and global hydrological models (GHMs) give different estimates. Wisser et al. (2008) showed that the discrepancies in the estimation stem from both meteorological and

ESDD
6, 81–132, 2015

irrigated area data. Recently, the Inter-Sectoral Impact Model Intercomparison Project (ISI-MIP) set the estimation of uncertainties in both GCMs and GHMs through inter-model comparison as one of its goals (Warszawski et al., 2014).

GCM biases are one of the substantial sources of uncertainty in future climate projections. For over a decade, we have made considerable effort to remove GCM biases from the temperature and precipitation data because these meteorological elements are crucial for analyzing the impact of climate change. However, hydrological simulations require other meteorological elements in addition to these elements. Solving water and heat budgets at the ground surface basically requires seven meteorological elements (atmospheric temperature, precipitation, short- and longwave downward radiation, wind velocity, pressure and humidity). Less attention has been paid to GCM biases of the other meteorological elements than to temperature and precipitation. Haddeland et al. (2012) intensively examined the compound effects of the bias correction of radiation, wind and humidity, and showed that bias correction has an impact on absolute values of evapotranspiration but less impact on relative changes. The ISI-MIP has provided meteorological data sets that were adjusted by a sophisticated bias correction method developed by Hempel et al. (2013). Although most of the meteorological elements used in GHMs were corrected by this method, the relative humidity remains uncorrected. It is important to quantitatively evaluate the size of the humidity biases existing in the original GCM data and the extent to which they affect the estimation of irrigational water. Moreover, global humidity data sets contain uncertainties originating from the accuracy of measurements, grid sampling (Willett et al., 2013) and the spatial variability within a land cell. The sensitivity of irrigational water to humidity conditions at different locations would help clarify the maximum expected uncertainty ranges in the estimation of irrigational water and their geographical susceptibility.

In this study, we examine possible uncertainty sources in estimating irrigational water abstraction by focusing on the propagation of uncertainties in humidity data. We also examine whether uncertainties in irrigational water abstraction across GCMs can be reduced if bias correction is applied to the humidity.

ESDD
6, 81–132, 2015

The data and analysis methods are described in Sect. 2 and the results and discussion are given in Sects. 3 and 4, respectively.

2 Data and methods

2.1 Bias-corrected meteorological data

We used bias-corrected meteorological data sets distributed by the ISI-MIP for driving GHM H08 (details of the model are given in Sect. 2.2). Five GCMs based on the Coupled Model Intercomparison Project Phase 5 (CMIP5) were used: GFDL-ESM2M (NOAA Geophysical Fluid Dynamics Laboratory), HadGEM2-ES (Met Office Hadley Centre with contribution by Instituto Nacional de Pesquisas Espaciais), IPSL-CM5A-LR (Institut Pierre-Simon Laplace), MIROC-ESM-CHEM (Japan Agency for Marine-Earth Science and Technology, Atmosphere and Ocean Research Institute (The University of Tokyo) and National Institute for Environmental Studies) and NorESM1-M (Norwegian Climate Centre). Hereafter, we abbreviate these GCMs to GFDL, HadGEM, IPSL, MIROC and NorESM, respectively. Bias correction was applied to the meteorological elements listed in Table 1 using the method of Hempel et al. (2013) with observation-based WATCH meteorological data sets (Weedon et al., 2011) for 1960–1999. The bias in relative humidity in the GCMs has remained uncorrected because of difficulties in preserving physical consistency between humidity-related variables (relative/specific humidity, vapor pressure), the atmospheric temperature and the pressure after bias correction (ISI-MIP, 2012). The geographical resolution of all meteorological data is commonly adjusted to $0.5^{\circ} \times 0.5^{\circ}$. Future projections were made under four representative concentration pathways (RCPs 2.6, 4.5, 6.0 and 8.5) (Moss et al., 2010; van Vuuren et al., 2011).

ESDD
6, 81–132, 2015

2.2 Hydrological model

The hydrological model used in this study was H08 (Hanasaki et al., 2008a, b). The model solves both the water and energy balances at a time step of one day with global coverage at a resolution of 0.5° × 0.5°. The model consists of six submodels (land surface hydrology, river routing, crop growth, water abstraction, reservoir operation and environmental flow requirement), but only the first four submodels were employed in this study. The land surface hydrology submodel solves the water and energy balances. The submodel solves the water balance using simple and basic physical hydrological processes that are suitable for global-scale simulation. A 1 m leaky bucket is assumed in the model: the soil moisture in each land cell is expressed as water stored in this bucket, and the water slowly drains from the bucket to express the subsurface runoff. The crop growth submodel is a process-based model. The human impacts of irrigational, municipal and industrial water abstraction from rivers for consumptive use were determined. To stabilize the initial conditions, the hydrological model was spun up using data from 1950 to 1959.

We assumed that irrigational water is supplied to irrigated cropland under the condition that crops are not affected by water stress. The soil water content is maintained at 75 % of the field capacity for all crops except rice (100 %) during the growing season and for 30 days before the planting date. The soil water of cropland is lost through evapotranspiration and runoff. The former is estimated by solving the energy balance at the land surface, whereas the latter varies with the soil water content. The spatial distribution of the irrigated area is fixed at that for the year 2000 based on the data of Siebert et al. (2005) throughout the analysis period. We separately calculated the results for four different water management schemes corresponding to four types of land use: double-cropping irrigated cropland (we refer to this water management scheme as Mosaic 1 hereafter), single-cropping irrigated cropland (Mosaic 2), rain-fed cropland (Mosaic 3) and other uses (Mosaic 4). Their geographical distributions are shown in

ESDD
6, 81–132, 2015

Fig. 1. We aggregated the four types of water management into a land cell (Mosaic 0) in consideration of their areal fractions in each land cell.

In this study, we evaluated two quantities regarding the irrigational water (the water volume is reported on a water withdrawal basis, not on a consumption basis): irrigational water demand (IWD) and simulated irrigation water abstraction from rivers (IWAR). The former gives the maximum potential water abstraction while maintaining the current agricultural maneuver (geographical distribution of irrigated cropland, cultivars, water management in irrigated cropland, etc.) under idealized conditions without fear of water shortage. The latter gives simulated irrigational water abstraction under the constraints of water availability from river flow. For both IWD and IWAR, we take the irrigation efficiency (the ratio of water supplied to cropland to abstracted water) into account because a certain proportion of water is lost after abstraction from rivers but before reaching cropland. The efficiency summarized in Döll and Siebert (2002) was used.

2.3 Evapotranspiration calculation scheme

Up to now, various formulae for estimating potential evapotranspiration have been developed (e.g. Shelton, 2009), and researchers have utilized suitable formulae for their own research purposes. These formulae are classified into two basic categories: physical and empirical formulae. The former describes potential evapotranspiration from the viewpoint of the energy balance at the land surface, and such formulae are suitable for (micro-)meteorological studies requiring a high temporal resolution. Thus, this type of formula requires several meteorological elements such as the surface temperature, humidity, radiation, and wind speed. On the other hand, the latter describes climatological conditions for less time-varying phenomena in a simplified manner and, in general, requires only two or three meteorological elements. Thus, the latter is suitable for sites where meteorological observation data are limited. Examples of evapotranspiration formulae are given in the Appendix.

ESDD
6, 81–132, 2015

The calculation scheme for potential evapotranspiration E_{pot} employed in H08 is the bulk formula (Kondo, 1994)

$$E_{pot} = \rho C_D U(q_{sat}(T_s) - q), \quad (1)$$

where ρ, C_D and U are the air density, bulk transfer coefficient (= 0.003) and wind speed, respectively. Thus, E_{pot} is proportional to the difference between the saturated specific humidity at the surface temperature $q_{sat}(T_s)$ and the specific humidity of the air q. Since bias correction was independently applied to each meteorological element except for the relative humidity, the physical consistency among meteorological elements guaranteed in the original GCMs might be lost. In this study, we recalculated q to maintain local physical consistency between the bias-corrected temperature and uncorrected relative humidity.

Actual evapotranspiration is estimated by multiplying by a function of the soil water content W. If W is less than three-quarters of the field capacity W_{fc}, E_{act} linearly decreases with decreasing W:

$$E_{act} = \beta E_{pot}, \quad (2)$$

where

$$\beta = \begin{cases} 1 & (W \geq 0.75W_{fc}) \\ \frac{W}{0.75W_{fc}} & (W < 0.75W_{fc}) \end{cases}. \quad (3)$$

As described earlier, since we assumed that the soil water content in irrigated cropland is maintained at $0.75W_{fc}$ during the growing season, $E_{act} = E_{pot}$ is always satisfied.

2.4 Experiment design of this study

To investigate the effects of bias correction of the humidity, we designed three sets of experiments in this study: (1) a reference experiment, (2) a sensitivity experiment and

ESDD
6, 81–132, 2015

(3) a bias-corrected experiment. In the reference experiment, a hydrological simulation was performed with the uncorrected humidity data described in Sect. 2.1. We evaluated the evapotranspiration and irrigational water for both present and future periods. The results were also used as a reference for the other two sets of experiments, details of which are given below.

2.4.1 Sensitivity experiment with hypothetical bias in humidity

Measurement of the atmospheric humidity inevitably involves errors. Observation-based humidity data sets, which are often used as reference data for bias correction, might contain a certain level of error. Moreover, the sensitivity of the amount of irrigational water to atmospheric humidity varies geographically or seasonally because irrigational water depends not only on meteorological conditions but also on the areal fraction of irrigated cropland and the cultivation maneuver (crop type, crop calendar, etc.) in each land cell.

To evaluate the sensitivity of the amount of irrigational water to atmospheric humidity, we carried out a sensitivity experiment in which we introduced a pair of constant biases so that the data were higher and lower than the original GCM-based humidity data and investigated the effect of the biases on irrigational water. The sensitivity is also helpful for predicting the size of the error in the simulation of irrigational water. In this experiment, we introduced "hypothetical" biases into the relative humidity by simply adding biases of ±5 % RH as a worst case (discussed below) homogeneously to all the land cells. (Hereafter, to discriminate between the unit of relative humidity and a general percentage, we use % RH for the unit of humidity.) If the relative humidity exceeds 100 % RH or becomes negative, we use values of 100 and 0 % RH, respectively. The other meteorological elements are unchanged. This experiment was carried out for the present period.

In fact, Willett et al. (2013) reported that the maximum uncertainties in humidity measurements with dry- and wet-bulb thermometers amounted to 2.75 and 5 % RH at temperatures of 0 and −10 °C, respectively. Emeis (2010) summarized the errors for

ESDD
6, 81–132, 2015

various measurement equipment: for example, advanced equipment based on the capacitive method has an accuracy of 2 % RH (for a humidity of 10–80 % RH) to 3 % RH (for a humidity of 80–ca. 100 % RH). By considering these reports, we set ±5 % RH as the worst case in this study.

Through such sensitivity experiments, we are able to estimate the largest possible ranges of uncertainty in irrigational water abstraction due to an uncertainty in the relative humidity of α % RH because the uncertainty for irrigational water in the case of geographically random biases within $\pm\alpha$ % RH necessarily lie between those for the two extremes of the globally homogeneous bias of $\pm\alpha$ % RH. Recall that $E_{act} = E_{pot}$ for irrigated cropland during the growing season. If we artificially add positive (negative) biases to the relative humidity without changing other elements, both ρ and $q_{sat}(T_s) - q$ on the right-hand side of the bulk formula (Eq. 1) decrease (increase), resulting in a decrease (an increase) in potential evapotranspiration. The increase in E_{pot} via $q_{sat}(T_s)$[1] is smaller than the direct decreasing effect on E_{pot} of introducing a hypothetical bias of α % RH. Therefore, E_{act} has a monotonic dependence on the humidity bias: E_{act} becomes smaller (larger) for positive (negative) biases in the relative humidity.

We note that this simple relation holds only for irrigated cropland during the crop growing season when irrigation water is supplied. In rain-fed cropland or irrigation-free seasons, evapotranspiration has a complex dependence on meteorological conditions (Wang and Dickinson, 2012) because E_{act} also depends on the soil moisture content (Eq. 3).

2.4.2 Bias-corrected experiment

If we introduce bias correction of the humidity, does it affect hydrological projections and have any advantages? To examine this effect, we prepared another set of meteorolog-

[1] A decrease (an increase) in potential evapotranspiration will increase (decrease) T_s owing to the prevention (promotion) of cooling by latent heat, and result in an increase (a decrease) in E_{pot} through an increase (a decrease) in $q_{sat}(T_s)$.

ESDD
6, 81–132, 2015

ical data for which the humidity data were bias-corrected with a primitive methodology that adjusts only the monthly climatology. Using this bias-corrected humidity data set and the original bias-corrected meteorological data sets for the other elements, we recalculated the hydrological process in the same way and compared the results with the uncorrected ones (i.e. those of the reference experiment). This experimemt was carried out for both the present and future periods.

The bias-correction methodology was based on additive adjustment. First, we obtained the monthly climatological relative humidity at all land cells for each GCM by averaging the relative humidity data for the same month of the year over the period 1960–1999. By subtracting the monthly climatological relative humidity in the GCM for the same period from those in the WATCH observational data, we determined the climatological monthly adjustments. Then, we compiled daily bias-corrected humidity data by simply adding the climatological monthly adjustments to the original GCM daily humidity data. Values of less than 0 % RH and greater than 100 % rh were set to 0 and 100 % RH, respectively.

3 Results

3.1 Performance of meteorological elements between GCMs

We first examine the differences in the meteorological elements between the five GCMs in the framework of the reference experiment to search for existing GCM-inherent biases and compare them with the WATCH observation-based meteorological elements to evaluate the performance of bias correction. Figure 2 shows the monthly difference worldwide averaged over each type of land use (mosaic). Monthly profiles of the atmospheric temperature, precipitation and shortwave downward radiation for the five GCMs agree with those of WATCH. Note that the 30 year analysis period (1971–2000) is slightly different from the bias correction period (1960–1999). For the wind speed data, although the monthly profile of MIROC is slightly larger than that of WATCH over

ESDD
6, 81–132, 2015

Mosaic 1, we consider the overall performance of bias correction to be reasonably good for the wind data.

In contrast, the monthly profiles of the relative humidity, which contain GCM-inherent biases, show a large dispersion between the five GCMs and also deviate from those of WATCH. Mosaic 1 has a larger dispersion than the other mosaics: the largest difference in the relative humidity between the monthly GCMs reaches 19.8 % RH in both January and October with a minimum of 11.0 % RH in May for Mosaic 1.

Such differences in the uncorrected relative humidity cause the deviation of the potential evapotranspiration and evapotranspiration between the five GCMs. Figure 3 shows their monthly profiles. Different GCMs have different monthly profiles and peak months. The difference in the potential evapotranspiration among the GCMs for Mosaic 1 reaches a maximum of 1.23 mm day^{-1} in June with a minimum of 0.56 mm day^{-1} in December. The difference exceeds 0.9 mm day^{-1} from March to October. Since the temperature, shortwave downward radiation and wind speed, which are required for the calculation of the potential evapotranspiration (Eq. 1), are successfully bias-corrected (Fig. 2), these differences in the potential evapotranspiration are considered to be mainly due to GCM biases in the relative humidity. NorESM tends to have a small but positive bias of the potential evapotranspiration and a small negative bias of the evapotranspiration during the summer. However, no clear biases of the relative humidity can be observed in Fig. 2.

Next, we determine the geographical distribution of the GCM biases with respect to the WATCH data because regional deviations with opposite signs may cancel each other when calculating the global mean. Figures 4 and 5 show the SD of 12 month climatological data of the relative humidity and atmospheric temperature with respect to the WATCH data, respectively. Strong regional patterns were detected in the relative humidity (Fig. 4). Figure 4 also shows that the relative humidity in high mountainous areas (Rocky, Andes and Himalayas) have larger deviations from the WATCH data for all GCMs. Each GCM has a different geographical distribution. For example, GFDL exhibits large differences over the world. HadGEM and IPSL have large differences

ESDD
6, 81–132, 2015

in Eurasia but good performance in Australia. MIROC has high deviations in inland regions of Asia and Australia. NorESM has small differences in Europe and Eastern United States but large differences in Australia.

In contrast, uniformly distributed small biases (less than 0.5 °C for most of the world) were observed for the temperature (Fig. 5). These results also indicate that the bias correction of the atmospheric temperature was successful at the regional scale.

We averaged the monthly SD over the land cells of each mosaic and summarize the results in Table 2. As expected from Fig. 4, HadGEM has the smallest deviation from WATCH over all land cells (Mosaic 0). However, MIROC and NorESM have superior performance for Mosaics 1 and 2. Since both Mosaics 1 and 2 are irrigated cropland, differences in the potential evapotranspiration directly affect differences in the amount of irrigational water. That is, small humidity biases over irrigated cropland are beneficial for suppressing their effects on irrigational water.

3.2 GCM features and their propagation into future projections

Next, we examine the extent to which GCM-inherent features in the relative humidity affect the estimation of irrigational water and propagate into a future period (2070–2099) in the framework of the reference experiment. If the effects are not negligible, bias correction of the humidity, as well as other meteorological elements, is highly recommended. To easily perceive the differences between the GCMs, we evaluate the relative anomaly of the five GCMs with respect to their ensemble mean. The results of anomalies in the relative humidity and related hydrological elements (potential evapotranspiration, evapotranspiration, IWD and IWAR) are shown in Figs. 6 and 7.

First, Fig. 6 shows that the monthly anomaly profiles of the potential evapotranspiration, evapotranspiration and IWD are similar but vertically opposite those of the relative humidity. This relation is expected from Eq. (1) while other meteorological conditions are fixed. We note that although the evapotranspiration from rain-fed cropland (Mosaic 3) also depends on the soil moisture, GCM-inherent features are weakly observed in the monthly profile of evapotranspiration.

ESDD
6, 81–132, 2015

Second, Fig. 7 shows that the future monthly anomaly profiles of the relative humidity are very similar to the present ones (Fig. 6) for all GCMs. This implies that the GCM-inherent biases propagate into future projections. As a result, the future monthly profiles of other hydrological elements also resemble the present ones.

Since IWAR is limited by the availability of riverine water, GCM-inherent features are weakened but remain. For example, larger positive anomalies in HadGEM and IPSL and negative ones in MIROC during boreal fall for 1971–2000 (Fig. 6) are similarly observed in the future projections (Fig. 7).

3.3 Uncertainties in absolute values of irrigational water across GCMs

In Table 3a and b, we summarize the results of the reference experiment on present and future values of the global sum of irrigational water, focusing on their ranges across the GCMs. Note that the global sum of irrigational water (Mosaic 0) is equivalent to the sum of those for Mosaics 1 and 2 because no irrigation is applied to Mosaics 3 and 4. IWD ranges between 2809.0 and 3554.9 $km^3 yr^{-1}$ for 1971–2000. A larger increase of 20 % or more in the future (2070–2099) is projected under a higher concentration of greenhouse gases such as under RCP 8.5. Both absolute values and relative changes show a large dispersion between the GCMs.

The present IWAR ranges between 1217.7 $km^3 yr^{-1}$ for NorESM and 1341.3 $km^3 yr^{-1}$ for IPSL. Since it is difficult to validate these results with observed data because of the lack of global census data, we compare the results with those in previous studies. Wada et al. (2013) reviewed past studies on irrigational water consumption (in their Table S1), which was in the range of 1029–1772 $km^3 yr^{-1}$ at the end (or the last few decades) of the 20th century. Rost et al. (2008) reported that global blue water consumption for irrigational use was 1364 $km^3 yr^{-1}$ when contributions from fossil groundwater and diverted rivers were neglected. Our estimations of IWAR are close to these reported results.

In contrast to IWD, future changes in IWAR relative to the 1971–2000 values show a small increase of at most 4.4 %. Several pairs of GCM-RCPs show a small decrease

ESDD
6, 81–132, 2015

in the future. Since IWAR is strongly constrained by water availability from rivers, these results reflect the future river flow. In other words, current irrigational maneuvers cannot be sustained by only riverine water under a future warming climate for these scenarios because, despite increasing demand for irrigational water (Table 3a), water abstraction from rivers cannot meet the demand (Table 3b) at the global scale.

We note that MIROC and NorESM, whose relative humidity shows small deviations from the observation (see Sect. 3.1), tend to have the smallest IWD and IWAR values among the five GCMs.

Monthly profiles of the global sum of the present and future IWAR (Fig. 8) differ among the GCMs. Since most irrigated croplands are distributed in the Northern Hemisphere, the global sum of IWAR has a peak in boreal summer of approximately three times the value in boreal winter. Despite large differences in the absolute monthly values between the GCMs, all GCMs show a future increase in IWAR in boreal summer and a decrease in boreal spring under a future warmer climate. Although in April, the global sum of the future IWD is approximately the same as that of the present IWD (not shown), the future IWAR is expected to decrease in boreal spring (Fig. 8). This result indicates that the future decrease in IWAR is attributable to a deficit in irrigational water that can be abstracted from rivers, not to an increase in evapotranspiration demand from cropland.

3.4 Sensitivity experiment with hypothetical biases

We investigate the effect of humidity biases on irrigational water by examining the results of the sensitivity experiment by adding biases of ±5 % RH homogeneously all over the world. Table 4a and b show that biases of ±5 % RH approximately correspond to changes in IWD of ±6.5 to ±7.5 % and IWAR of ±3.5 to ±4.5 % (or ±50 $km^3 yr^{-1}$) as the maximum error range. Monthly profiles of IWAR with biased humidity also deviate from the original profiles (Fig. 9). The effect of the artificial bias is clearly observed during boreal summer. Comparing Tables 3a, b and 4a, b or Figs. 8 and 9, changes

ESDD
6, 81–132, 2015

with ±5 % RH biases are comparable to, or sometimes larger than, future changes in IWAR under RCP 8.5.

Figure 10 shows the geographical distribution of the sensitivity (i.e. the change in IWD or IWAR per unit change in the relative humidity (1 % RH)) for June and August. The negative sensitivity of IWD, as expected from Eq. (1), is observed, particularly in India and East China, where both double-cropping and single-cropping irrigated croplands are intensely distributed. In contrast, midlatitudes (Europe to Central Asia and North America) show smaller negative sensitivity than India and East China. This implies that IWD in India and East China is more sensitive to small changes in the relative humidity than other regions of the world, possibly due to the high temperature in summer and the high areal fraction of irrigated cropland.

The sensitivity of IWAR shows a similar geographical distribution to that of IWD but with a smaller magnitude. In June, the negative sensitivity of IWAR is markedly weaker than that of IWD in India and East China. These features are considered to be due to the limited water availability in river flow, which results in less dependence on the atmospheric humidity. In fact, the rainy season starts in June in India and in June and July in southern and northern China, respectively.

From these results, to effectively and efficiently reduce the uncertainty of irrigational water abstraction, more stringent accuracy for the atmospheric humidity data is required for India and East China.

3.5 Bias-corrected experiment and effects of reduction of uncertainty across GCMs

Next, we examine the extent to which uncertainties are reduced by bias correction of the humidity data (Sect. 2.4.2). Figure 11 shows monthly anomalies of hydrological elements with respect to the GCM-ensemble means. In comparison with Fig. 6, the relative humidity of all GCMs are in good agreement, implying that bias correction, even with a primitive method, is effective. The potential evapotranspiration is also similar among the GCMs except for NorESM, which has a positive bias. NorESM also had a posi-

ESDD
6, 81–132, 2015

tive bias in Fig. 3. The monthly profiles of the evapotranspiration, IWD and IWAR are confined in narrower ranges than those for the uncorrected humidity data. For example, IWD remains within ±20 % from the ensemble mean throughout the year, in clear contrast to the range of approximately ±30 % in Fig. 6. Future projections (Fig. 12, in comparison with Fig. 7) also show the advantageousness of reducing differences in projected hydrological elements across the GCMs by bias correction of the humidity data.

Bias correction of the humidity data also reduces the uncertainties (i.e. the range between the maximum and minimum) in the monthly IWD and IWAR for the five GCMs (Fig. 13). Hereafter, the monthly reduction in uncertainties is quantified as the ratio of the range with bias-corrected humidity data to that with uncorrected humidity data for IWD and IWAR. For 1971–2000, the range of IWD projected with the bias-corrected humidity data is smaller than that with the uncorrected data: the range of the uncorrected data is 11 % for the best month (January) and 83 % for the worst month (May). Even for future projections under RCP 8.5, the range of IWD with the bias-corrected data is 32 % (best month, January) to 88 % (worst month, June) of that with the uncorrected data. The results for IWAR, which is governed by riverine water availability, also suggest the advantageousness of bias correction of the humidity data: for 1971–2000, the range of IWAR with the bias-corrected data is reduced to as little as 29 % of that with the uncorrected data (December), although the range is increased in June and July (114 and 105 %, respectively).

The reduction in uncertainty by bias correction of the humidity was also clearly observed in the absolute annual values of IWD and IWAR. Table 5 shows the annual values of IWD and IWAR and their ranges across the GCMs. The uncertainty ranges with bias-corrected humidity data (bottom line), in comparison with those in Table 3a and b, are reduced from 745.9 to 426.1 $km^3 yr^{-1}$ and from 123.6 to 98.6 $km^3 yr^{-1}$ for the present IWD and IWAR, respectively. Similarly, the range decreases from 971.8 to 544.0 $km^3 yr^{-1}$ and from 119.9 to 77.6 $km^3 yr^{-1}$ for future (RCP 8.5, 2070–2099) projections of IWD and IWAR, respectively. Absolute values estimated using a single GCM

ESDD
6, 81–132, 2015

were also affected by bias correction of the humidity. For example, IPSL shows a large reduction in IWD as a result of bias correction. This indicates that the large IWD values for IPSL in Table 3a and b can be attributed to biased humidity data.

4 Discussion

4.1 Necessity of bias correction of humidity data

It is widely known that bias correction is necessary for hydrological simulations with GCM meteorological data because the raw meteorological outputs of GCMs deviate from meteorological observations. The probability density functions of meteorological elements generated by GCMs for a past period often deviate from those of observed elements (e.g. Piani et al., 2010a, b). Since these GCM-inherent features in the humidity affect other hydroclimatological elements and propagate in future projections, we are convinced that bias correction of the humidity, as well as the atmospheric temperature and precipitation, is crucial for analyzing the impact of climate change and also beneficial for dampening GCM-inherent features in projections of evapotranspiration and irrigational water abstraction.

Owing to the successful removal of GCM biases except for humidity by employing a state-of-the-art methodology (Hempel et al., 2013) (Fig. 2), we can focus on the effects of GCM biases in the humidity in this study. Since the GCM biases are negligible in other meteorological elements (such as temperature and precipitation), we consider that the differences in future projections of evapotranspiration and irrigational water abstraction (Figs. 6 and 7) among GCMs are primarily attributable to GCM biases in the relative humidity.

Although considerable attention has been paid to GCM biases in the temperature and precipitation, less attention has been paid to GCM biases in the humidity. A pioneering study by Haddeland et al. (2012) examined the compound effects of bias corrections of shortwave and longwave radiation, humidity and wind, in contrast to

ESDD
6, 81–132, 2015

our analysis focusing on the bias correction effects of humidity. They compared hydrological simulations driven by bias-corrected and uncorrected meteorological data and showed that bias correction of radiation, humidity and wind speed increases the agreement with baseline simulations. They also pointed out that bias correction significantly affects the absolute values of simulated runoff and evapotranspiration. In this sense, our results are in agreement with their results. On the other hand, they used four GHMs implementing different potential evapotranspiration formulae (see also Appendix); three of them, LPJmL, WaterGAP (Priestley–Taylor) and MPI-HM (Thornthwaite), are empirical-type formulae that are independent of the atmospheric humidity. Only VIC (Penman–Monteith) is a physical type and dependent on the humidity. Thus, we consider that GHMs with empirical formula are insensitive to uncertainties in humidity data. We will discuss the problem of the GHM dependence on humidity data from a different viewpoint in the next subsection.

Figure 10 implies that the high sensitivity of humidity data over India and East China plays a key role in the uncertainty in the global sum of irrigational water. In these regions, the areal fraction of irrigated cropland is higher than in other regions. Even if the evapotranspiration over a unit area of irrigated cropland was the same over the globe, the total amount of water loss via evapotranspiration over a unit land area would be larger over densely distributed irrigated cropland than over sparsely distributed irrigated cropland. Moreover, the potential evapotranspiration has higher sensitivity to the atmospheric humidity at higher temperatures than at lower temperture; since air is able to contain more vapor at higher temperatures, the vapor pressure deficit for a given relative humidity is also larger at higher temperatures.

Moreover, in both India and East China, since future water availability is expected to worsen in these regions owing to an increase in the population and increasing demand for agricultural production, it is highly desirable to accurately estimate future water demand. Some studies (Wada et al., 2010, 2012) have warned that a large volume of irrigational water in excess of recharge is being abstracted from groundwater in India. Water availability is determined by the balance between water supply and demand. Re-

ESDD
6, 81–132, 2015

ducing the uncertainties in future projections of irrigational water demand, as well as other factors such as future socio-economic scenarios and agricultural maneuvers, will help obtain reliable estimates of future water availability. This statement also applies to monthly water availability. In fact, some studies have shown that water availability (or water stress) varies from month to month (Hoekstra et al., 2012; Hanasaki et al., 2013).

4.2 Caveats on different sensitivities of evapotranspiration to atmospheric humidity

In climate impact studies on evapotranspiration, since GCM outputs are used as GHM inputs, both GCMs and GHMs may be sources of intermodel differences. Different evapotranspiration formulae adopted in different GHMs may be a source of differences in evapotranspiration among GHMs. The performance of the various evapotranspiration formulae that have been proposed has been primarily examined in comparison with the results of in situ observation (e.g. Winter et al., 1995; Federer et al., 1996; Vörösmarty et al., 1998; Lu et al., 2005; Rao et al., 2011) at various geographical scales. As described in Sect. 2.3 and the Appendix, evapotranspiration formulae are classified into physical and empirical formulae. In practice, since the former formulae require more meteorological elements (e.g. wind, humidity, etc.) than the latter, the availability of observed meteorological data is the key to choosing which type of potential evapotranspiration formula to implement.

Existing these two types of potential evapotranspiration formula indicates that GHMs implementing physical potential evapotranspiration formulae (referred to as phGHMs hereafter) are sensitive to the atmospheric humidity, whereas GHMs implementing empirical formulae (emGHMs hereafter) are insensitive to the humidity. Thus, uncertainties in the humidity affect phGHMs but not emGHMs.

Recently, studies on irrigational water published as ISI-MIP Fast Track results have reported future changes in its seasonality (Wada et al., 2013) and the possibility of reduced water availability in river basins due to increasing demand for irrigational water (Haddeland et al., 2014). In both papers, the authors reported that there are large

ESDD
6, 81–132, 2015

differences in the future projections of hydrological elements among the GHMs. As summarized in Huber et al. (2014), the next impact studies should explore the reasons for intermodel differences to better understand the mechanisms underlying the impact of climate change. However, since each GHM is an assemblage of software modules, every scheme and parameter adopted in each GHM may be a source of intermodel differences. For example, as tabulated in Table S3 of Wada et al. (2013), intermodel differences in the global sum of irrigational water withdrawal among the GHMs are ascribed to differences in not only the evapotranspiration but also the total area of irrigated cropland adopted in the GHMs. We are a long way from identifying possible sources of intermodel differences.

To examine the contributions to uncertainty from smaller components of software, we can take top-down and bottom-up approaches. In the former approach, we first evaluate the overall differences, then we allocate them into smaller differences originating from smaller components of software modules. One example of this approach can be seen in Wada et al. (2013), who classified the overall uncertainties into three possible sources (GHMs, GCMs and RCPs) based on the method of Hawkins and Sutton (2009). In the latter approach, as shown in this study, we first obtain differences generated by a single software component and estimate their overall differences. This is laborious but advantageous for identifying contributions from each component or from the calculation process.

We note that a special care should be taken to account for the different sensitivity to the humidity between phGHMs and emGHMs when using a top-down approach. For example, if we deal with both phGHMs and emGHMs together without special care, GCM-inherent humidity biases can be misinterpreted as GHM-inherent features because of the different sensitivity to the humidity.

ESDD
6, 81–132, 2015

4.3 Other factors contributing to uncertainty in future projections of hydroclimatological environments

Evapotranspiration plays a key role in global water circulation (Oki and Kanae, 2006; Trenberth et al., 2011). Under global warming, the global hydrological cycle is considered to be strengthened owing to intensified precipitation and increasing evapotranspiration. The global energy cycle (Trenberth et al., 2009; Stephens et al., 2012) can be changed by changes in the hydrological cycle via latent heat transported by water vapor flux. It has been a matter of controversy whether the surface humidity will change with climate change. Dai (2006) found that the relative humidity averaged over the global land area remained almost constant during 1976–2004, whereas the specific humidity increased owing to the increasing surface temperature. Willett et al. (2007) showed that the significant increase in surface specific humidity is mainly attributable to human influence by performing a detection-and-attribution analysis. If the climatological relative humidity changes in the future, we should also consider its effects on assessments of the impact of climate change by applying a suitable methodology for bias correction.

We consider that, in a practical sense, bias correction is still necessary for analyzing the impact of climate change to remove GCM-inherent biases. Ehret et al. (2012) posed the controversial but important question of whether we should prioritize the application of bias correction to meteorological inputs because most bias correction methodologies independently correct biases of different elements without considering their mutual physical relations. In fact, as described in Sect. 2.1, humidity-related variables are strictly linked to the atmospheric temperature (and pressure). Moreover, the atmospheric humidity closely interacts with weather conditions (e.g. the humidity is high on rainy days). In this study, sacrificing stringency, we attempted to adjust the monthly climatology of the relative humidity by applying a primitive additive bias correction (Sect. 2.4.2). Even without an advanced methodology, bias correction of the humidity is advantageous in reducing uncertainties in irrigational water across the GCMs. The development of next-generation methodologies of bias correction with physical consis-

ESDD
6, 81–132, 2015

tency among meteorological variables would greatly increase the reliability of future projections of hydroclimatological environments.

Although we primarily focused on irrigational water in this study, we did not fully discuss the reduction in evapotranspiration caused by a low soil water content (see Eq. 2) in an explicit manner. Future changes in global evapotranspiration, including those in areas of rain-fed cropland and natural vegetation, require a more complex discussion because evapotranspiration is determined by not only atmospheric conditions but also soil moisture conditions, which vary with the soil properties and topography. However, the latter has higher geographical diversity than the former because of the dependence on topographical and geological conditions. The in situ observation of soil moisture often shows significant differences at two sites separated by a small distance (Masaki et al., 2011). Jung et al. (2010) showed that the declining trend in global land evapotranspiration since 1998 is attributable to limited soil moisture.

Changes in land use (e.g. transition to irrigated cropland), which are not considered in this study nor in the ISI-MIP Fast Track results, also alter the regional water flux between the land and the atmosphere (Gordon et al., 2005). However, such anthropogenic effects are highly dependent on future socio-economic scenarios, which still contain large uncertainties. If future changes in land use are large, we cannot neglect the feedback process from the land to the atmosphere, and the validity of offline simulation (i.e. GHMs able to run separately with GCMs), which is frequently used in climate impact studies, might become limited.

5 Conclusions

We have quantitatively investigated the propagation of uncertainties in humidity data into the estimation of the amount of irrigational water under ongoing climate change. We used bias-corrected meteorological data sets (except for the atmospheric humidity) of five GCMs distributed by the ISI-MIP. We used H08 for hydrological simulation at the global scale for both present and future periods under four RCPs. H08 employs the

ESDD
6, 81–132, 2015

bulk formula, which is sensitive to the atmospheric humidity, to calculate the potential evapotranspiration.

The monthly relative humidity of the five GCMs deviated from the observed meteorological data sets (WATCH) by up to ca. 20 % RH for 1970–2000 over global land cells (Mosaic 0). Monthly profiles of the relative humidity show the characteristics of each GCM, which propagate into monthly profiles of hydrological elements such as evapotranspiration and irrigational water demand obtained by both historical and future simulations. The global sums of irrigational water demand (IWD) and irrigational water abstraction from rivers (IWAR), where the latter is constrained by riverine water availability, were evaluated as a reference when we used uncorrected humidity data. The obtained values were widely spread from 2809.0 to 3554.9 $km^3 yr^{-1}$ (range = 745.9 $km^3 yr^{-1}$) for IWD and from 1217.7 to 1341.3 $km^3 yr^{-1}$ (123.6 $km^3 yr^{-1}$) for IWAR between the five GCMs for the present period (1971–2000). Estimations of IWD and IWAR under RCP 8.5 (2070–2099) varied from 3250.2 to 4222.0 $km^3 yr^{-1}$ (971.8 $km^3 yr^{-1}$) and from 1234.8 to 1354.7 $km^3 yr^{-1}$ (119.9 $km^3 yr^{-1}$) between the GCMs, respectively.

A sensitivity experiment involving the uniform addition of hypothetical biases of ±5 % to the humidity data over all land areas showed that the hypothetical biases cause the global sum of IWAR to deviate by ca. 50 $km^3 yr^{-1}$ in the worst case. High sensitivity to bias was observed in India and East China, where intensified irrigated cropland is distributed, during the crop-growing season.

We also found that the bias correction of humidity data can reduce uncertainties in the estimation of IWD and IWAR across the GCMs. Even for a primitive bias correction method which adjusts the monthly climatological humidity of each land cell, we observed a reduction in uncertainties. The ranges across the GCMs for the present and future (RCP 8.5) periods were reduced to 426.1 and 544.0 $km^3 yr^{-1}$ for IWD and 98.6 and 77.6 $km^3 yr^{-1}$ for IWAR, respectively. The absolute values obtained using a single GCM are also improved by the bias correction.

ESDD
6, 81–132, 2015

We conclude that GCM biases in the humidity propagate into the present and future estimation of hydroclimatological factors such as evapotranspiration and irrigational water. Bias correction of the humidity can reduce uncertainties in the estimation of irrigational water across the GCMs. The results indicate that it is desirable to apply bias correction to not only the atmospheric temperature and precipitation but also the humidity.

Reliable future projections for IWAR are crucial for future projections of water availability, particularly in water-limited regions where different purposes of water abstraction conflict with each other. People living in some river basins have been or will be obliged to make difficult decisions regarding the allocation for various purposes of water use in their society because of the increasing demand for water under limited riverine water availability.

Recently, many authors have pointed out the problem of uncertainties in assessing the impact of climate change through the research projects such as the ISI-MIP. It is not an easy task to identify possible uncertainty sources from a huge assemblage of models, calculation schemes and parameters. Investigations such as this study will be helpful for identifing sources of uncertainty underlying assessments on the impact of climate change. Although we have a long way to go, reducing the possible uncertainties in studies on the impact of climate change is necessary to obtain a better understanding of future hydroclimatological environments and is an important next step.

Appendix A: Potential evapotranspiration formulae

Many formulae for calculating the potential evapotranspiration E_{pot} have been proposed. The performance of these formulae has been examined in comparison with observed data at various spatial and temporal scales (e.g. Winter et al., 1995; Federer et al., 1996; Vörösmarty et al., 1998; Lu et al., 2005; Rao et al., 2011). Descriptions of these formulae are also given in these references and in Shelton (2009); however, here we give some examples of the two types of formulae (physical and empirical; see also

ESDD
6, 81–132, 2015

Sect. 4.2) that have been implemented in GHMs in studies on the impact of climate change (e.g. Wada et al., 2013; Haddeland et al., 2014; Schewe et al., 2014).

Physical formulae

Penman–Monteith

$$E_{\mathrm{pot}} = \frac{\Delta(R_{\mathrm{n}} - G) + \rho c_p (e_{\mathrm{sat}} - e) r_{\mathrm{a}}^{-1}}{\Delta + \gamma(1 + r_s r_{\mathrm{a}}^{-1})} \tag{A1}$$

Bulk

$$E_{\mathrm{pot}} = \rho C_D U \left(q_{\mathrm{sat}}(T_{\mathrm{s}}) - q\right) \tag{A2}$$

Empirical formulae

Priestley–Taylor

$$E_{\mathrm{pot}} = c \frac{\Delta}{\Delta + \gamma}(R_{\mathrm{n}} - G) \tag{A3}$$

Thornthwaite

$$E_{\mathrm{pot}} = 1.067 \Lambda \left(\frac{10\overline{T_{\mathrm{a}}}}{I}\right)^{A} \tag{A4}$$

where $I = \sum \left(\frac{\overline{T_{\mathrm{a}}}}{5}\right)^{1.514}$

Hamon

$$E_{\mathrm{pot}} = \frac{715.5 \Lambda e_{\mathrm{sat}}(\overline{T_{\mathrm{a}}})}{\overline{T_{\mathrm{a}}} + 273.2} \tag{A5}$$

The symbols used in these equations have the following meanings.

ESDD
6, 81–132, 2015

Δ	gradient of saturated vapor pressure curve vs. air temperature
R_n	net radiation
G	soil heat flux (sometimes ~ 0)
ρ	air density
c_p	specific heat
e	vapor pressure
X_{sat}	saturated condition of X
r_a	aerodynamic resistance to vapor transfer
γ	psychrometric constant
r_s	canopy resistance
C_D	bulk transfer coefficient (= 0.003)
U	wind velocity
q	specific humidity
T_s	surface temperature
c	empirical constant
Λ	daylight hours per day
$\overline{T_a}$	mean atmospheric temperature
A	third-order polynomials of I

Acknowledgements. We thank S. Emori, T. Yokohata and H. Shiogama (NIES) for helpful discussions. This research was supported by the Environment Research and Technology Development Fund (S-10) of the Ministry of the Environment, Japan.

This work has been conducted under the framework of the ISI-MIP. The ISI-MIP Fast Track project was funded by the German Federal Ministry of Education and Research (BMBF) with project funding reference number 01LS1201A. Responsibility for the content of this publication lies with the authors.

We acknowledge the World Climate Research Programme's Working Group on Coupled Modelling, which is responsible for CMIP, and we thank the climate modeling groups (listed in Sect. 2.1 of this paper) for producing and making available their model outputs. For CMIP, the US Department of Energy's Program for Climate Model Diagnosis and Intercomparison provides coordinating support and leads the development of software infrastructure in partnership with the Global Organization for Earth System Science Portals.

ESDD
6, 81–132, 2015

References

Dai, A.: Recent climatology, variability, and trends in global surface humidity, J. Climate, 19, 3589–3606, 2006. 102

Döll, P. and Siebert, S.: Global modeling of irrigation water requirements, Water Resour. Res., 38, 1037, doi:10.1029/2001WR000355, 2002. 87

Ehret, U., Zehe, E., Wulfmeyer, V., Warrach-Sagi, K., and Liebert, J.: HESS Opinions "Should we apply bias correction to global and regional climate model data?", Hydrol. Earth Syst. Sci., 16, 3391–3404, doi:10.5194/hess-16-3391-2012, 2012. 102

Emeis, S.: Measurement Methods in Atmospheric Sciences, In situ and Remote, Gebrüder Borntraeger Science Publishers, Stuttgart, Germany, 257 pp., 2010. 89

Federer, C. A., Vörösmarty, C., and Fekete, B.: Intercomparison of models for calculating potential evaporation in regional and global water balance models, Water Resour. Res., 32, 2315–2321, 1996. 100, 105

Gordon, L. J., Steffen, W., Jönsson, B. F., Folke, C., Falkenmark, M., and Johannessen, Å.: Human modification of global water vapor flows from the land surface, P. Natl. Acad. Sci. USA, 102, 7612–7617, doi:10.1073/pnas.0500208102, 2005. 103

Haddeland, I., Heinke, J., Voß, F., Eisner, S., Chen, C., Hagemann, S., and Ludwig, F.: Effects of climate model radiation, humidity and wind estimates on hydrological simulations, Hydrol. Earth Syst. Sci., 16, 305–318, doi:10.5194/hess-16-305-2012, 2012. 84, 98

Haddeland, I., Heinke, J., Biemans, H., Eisner, S., Flörke, M., Hanasaki, N., Konzmann, M., Ludwig, F., Masaki, Y., Schewe, J., Stacke, T., Tessler, Z. D., Wada, Y., and Wisser, D.: Global water resources affected by human interventions and climate change, P. Natl. Acad. Sci. USA, 111, 3251–3256, doi:10.1073/pnas.1222475110, 2014. 100, 106

Hanasaki, N., Kanae, S., Oki, T., Masuda, K., Motoya, K., Shirakawa, N., Shen, Y., and Tanaka, K.: An integrated model for the assessment of global water resources – Part 1: Model description and input meteorological forcing, Hydrol. Earth Syst. Sci., 12, 1007–1025, doi:10.5194/hess-12-1007-2008, 2008a. 86

Hanasaki, N., Kanae, S., Oki, T., Masuda, K., Motoya, K., Shirakawa, N., Shen, Y., and Tanaka, K.: An integrated model for the assessment of global water resources – Part 2: Applications and assessments, Hydrol. Earth Syst. Sci., 12, 1027–1037, doi:10.5194/hess-12-1027-2008, 2008b. 86

ESDD
6, 81–132, 2015

Hanasaki, N., Fujimori, S., Yamamoto, T., Yoshikawa, S., Masaki, Y., Hijioka, Y., Kainuma, M., Kanamori, Y., Masui, T., Takahashi, K., and Kanae, S.: A global water scarcity assessment under Shared Socio-economic Pathways – Part 2: Water availability and scarcity, Hydrol. Earth Syst. Sci., 17, 2393–2413, doi:10.5194/hess-17-2393-2013, 2013. 100

Hawkins, E. and Sutton, R.: The potential to narrow uncertainty in regional climate predictions, B. Am. Meteorol. Soc., 90, 1095–1107, doi:10.1175/2009BAMS2607.1, 2009. 101

Hempel, S., Frieler, K., Warszawski, L., Schewe, J., and Piontek, F.: A trend-preserving bias correction – the ISI-MIP approach, Earth Syst. Dynam., 4, 219–236, doi:10.5194/esd-4-219-2013, 2013. 84, 85, 98, 113

Hoekstra, A. Y., Mekonnen, M. M., Chapagain, A. K., Mathews, R. E., and Richter, B. D.: Global monthly water scarcity: blue water footprints versus blue water availability, Plos One, 7, e32688, doi:10.1371/journal.pone.0032688, 2012. 100

Huber, V., Schellnhuber, H. J., Arnell, N. W., Frieler, K., Friend, A. D., Gerten, D., Haddeland, I., Kabat, P., Lotze-Campen, H., Lucht, W., Parry, M., Piontek, F., Rosenzweig, C., Schewe, J., and Warszawski, L.: Climate impact research: beyond patchwork, Earth Syst. Dynam., 5, 399–408, doi:10.5194/esd-5-399-2014, 2014. 101

ISI-MIP: Fact sheet: bias correction in the ISI-MIP, available at: https://www.pik-potsdam.de/research/climate-impacts-and-vulnerabilities/research/rd2-cross-cutting-activities/isi-mip/for-modellers/isi-mip-fast-track/input-data/bias-correction/bias-correction-fact-sheet (last access: 26 January 2015), 2012. 85

Jung, M., Reichstein, M., Ciais, P., Seneviratne, S. I., Sheffield, J., Goulden, M. L., Bonan, G., Cescatti, A., Chen, J., de Jeu, R., Dolman, A. J., Eugster, W., Gerten, D., Gianelle, D., Gobron, N., Heinke, J., Kimball, J., Law, B. E., Montagnani, L., Mu, Q., Mueller, B., Oleson, K., Papale, D., Richardson, A. D., Roupsard, O., Running, S., Tomelleri, E., Viovy, N., Weber, U., Williams, C., Wood, E., Zaehle, S., and Zhang, K.: Recent decline in the global land evapotranspiration trend due to limited moisture supply, Nature, 467, 951–954, doi:10.1038/nature09396, 2010. 103

Kondo, J.: Meteorology of Hydrological Environment, Asakura Shoten, Tokyo, Japan, 368 pp., 1994. 88

Lu, J., Sun, G., McNulty, S. G., and Amatya, D. M.: A comparison of six potential evapotranspiration methods for regional use in the southeastern United States, J. Am. Water Resour. As., 41, 621–633, 2005. 100, 105

ESDD
6, 81–132, 2015

Masaki, Y., Ishigooka, Y., Kuwagata, T., Goto, S., Sawano, S., and Hasegawa, T.: Expected changes in future agro-climatological conditions in Northeast Thailand and their differences between general circulation models, Theor. Appl. Climatol., 106, 383–401, doi:10.1007/s00704-011-0439-3, 2011. 103

Moss, R. H., Edmonds, J. A., Hibbard, K. A., Manning, M. R., Rose, S. K., van Vuuren, D. P., Carter, T. R., Emori, S., Kainuma, M., Kram, T., Meehl, G. A., Mitchell, J. F. B., Nakicenovic, N., Riahi, K., Smith, S. J., Stouffer, R. J., Thomson, A. M., Weyant, J. P., and Wilbanks, T. J.: The next generation of scenarios for climate change research and assessment, Nature, 463, 747–756, 2010. 85

Oki, T. and Kanae, S.: Global hydrological cycles and world water resources, Science, 313, 1068–1072, doi:10.1126/science.1128845, 2006. 102

Piani, C., Haerter, J. O., and Coppola, E.: Statistical bias correction for daily precipitation in regional climate models over Europe, Theor. Appl. Climatol., 99, 187–192, doi:10.1007/s00704-009-0134-9, 2010a. 98

Piani, C., Weedon, G. P., Best, M., Gomes, S. M., Viterbo, P., Hagemann, S., and Haerter, J. O.: Statistical bias correction of global simulated daily precipitation and temperature for the application of hydrological models, J. Hydrol., 395, 199–215, doi:10.1016/j.jhydrol.2010.10.024, 2010b. 98

Rao, L. Y., Sun, G., Ford, C. R., and Vose, J. M.: Modeling potential evapotranspiration of two forested watersheds in the Southern Appalachians, Trans. Am. Soc. Agric. Biol. Eng., 54, 2067–2078, 2011. 100, 105

Rost, S., Gerten, D., Bondeau, A., Lucht, W., Rohwer, J., and Schaphoff, S.: Agricultural green and blue water consumption and its influence on the global water system, Water Resour. Res., 44, W09405, doi:10.1029/2007WR006331, 2008. 94

Schewe, J., Heinke, J., Gerten, D., Haddeland, I., Arnell, N. W., Clark, D. B., Dankers, R., Eisner, S., Fekete, B. M., Colón-González, F. J., Gosling, S. N., Kim, H., Liu, X., Masaki, Y., Portmann, F. T., Satoh, Y., Stacke, T., Tang, Q., Wada, Y., Wisser, D., Albrecht, T., Frieler, K., Piontek, F., Warszawski, L., and Kabat, P.: Multimodel assessment of water scarcity under climate change, P. Natl. Acad. Sci. USA, 111, 3245–3250, doi:10.1073/pnas.1222460110, 2014. 106

Shelton, M. L.: Hydroclimatology: Perspective and Applications, Cambridge University Press, Cambridge, UK, 426 pp., 2009. 87, 105

ESDD
6, 81–132, 2015

Siebert, S., Döll, P., Hoogeveen, J., Faures, J.-M., Frenken, K., and Feick, S.: Development and validation of the global map of irrigation areas, Hydrol. Earth Syst. Sci., 9, 535–547, doi:10.5194/hess-9-535-2005, 2005. 86

Stephens, G. L., Li, J., Wild, M., Clayson, C. A., Loeb, N., Kato, S., L'Ecuyer, T., Stackhouse Jr., P. W., Lebsock, M., and Andrews, T.: An update on Earth's energy balance in light of the latest global observations, Nat. Geosci., 5, 691–696, doi:10.1038/NGEO1580, 2012. 102

Trenberth, K. E., Fasullo, J. T., and Kiehl, J.: Earth's global energy budget, B. Am. Meteorol. Soc., 90, 311–323, doi:10.1175/2008BAMS2634.1, 2009. 102

Trenberth, K. E., Fasullo, J. T., and Mackaro, J.: Atmospheric moisture transports from ocean to land and global energy flows in reanalyses, J. Climate, 24, 4907–4924, doi:10.1175/2011JCLI4171.1, 2011. 102

van Vuuren, D. P., Edmonds, J., Kainuma, M., Riahi, K., Thomson, A., Hibbard, K., Hurtt, G. C., Kram, T., Krey, V., Lamarque, J.-F., Masui, T., Meinshausen, M., Nakicenovic, N., Smith, S. J., and Rose, S. K.: The representative concentration pathways: an overview, Climatic Change, 109, 5–31, doi:10.1007/s10584-011-0148-z, 2011. 85

Vörösmarty, C. J., Federer, C. A., and Schloss, A. L.: Potential evaporation functions compared on US watersheds: possible implications for global-scale water balance and terrestrial ecosystem modeling, J. Hydrol., 207, 147–169, 1998. 100, 105

Vörösmarty, C. J., Lévêque, C., Revenga, C., Bos, R., Caudill, C., Chilton, J., Douglas, E. M., Meybeck, M., Prager, D., Balvanera, P., Barker, S., Maas, M., Nilsson, C., Oki, T., and Reidy, C. A.: Fresh water, in: Ecosystems and Human Well-being: Current State and Trends, The Millennium Ecosystem Assessment Series Volume 1, edited by: Hassan, R., Scholes, R., and Ash, N., Island Press, Washington, D.C., USA, 165–207, 2005. 83

Wada, Y., van Beek, L. P. H., van Kempen, C. M., Reckman, J. W. T. M., Vasak, S., and Bierkens, M. F. P.: Global depletion of groundwater resources, Geophys. Res. Lett., 37, L20402, doi:10.1029/2010GL044571, 2010. 99

Wada, Y., van Beek, L. P. H., and Bierkens, M. F. P.: Nonsustainable groundwater sustaining irrigation: a global assessment, Water Resour. Res., 48, W00L06, doi:10.1029/2011WR010562, 2012. 99

Wada, Y., Wisser, D., Eisner, S., Flörke, M., Gerten, D., Haddeland, I., Hanasaki, N., Masaki, Y., Portmann, F. T., Stacke, T., Tessler, Z., and Schewe, J.: Multimodel projections and uncertainties of irrigation water demand under climate change, Geophys. Res. Lett., 40, 4626–4632, doi:10.1002/grl.50686, 2013. 94, 100, 101, 106

ESDD
6, 81–132, 2015

Wang, K., and Dickinson, R. E.: A review of global terrestrial evapotranspiration: Observation, modeling, climatology, and climatic variability, Rev. Geophys., 50, RG2005, doi:10.1029/2011RG000373, 2012. 90

Warszawski, L., Frieler, K., Huber, V., Piontek, F., Serdeczny, O., and Schewe, J.: The inter-sectoral impact model intercomparison project (ISI-MIP): project framework, P. Natl. Acad. Sci. USA, 111, 3228–3232, doi:10.1073/pnas.1312330110, 2014. 84

Weedon, G. P., Gomes, S., Viterbo, P., Shuttleworth, W. J., Blyth, E., Österle, H., Adam, J. C., Bellouin, N., Boucher, O., and Best, M.: Creation of the WATCH forcing data and its use to assess global and regional reference crop evaporation over land during the twentieth century, J. Hydrometeorol., 12, 823–848, 2011. 85

Willett, K. M., Gillett, N. P., Jones, P. D., and Thorne, P. W.: Attribution of observed surface humidity changes to human influence, Nature, 449, 710–712, doi:10.1038/nature06207, 2007. 102

Willett, K. M., Williams Jr., C. N., Dunn, R. J. H., Thorne, P. W., Bell, S., de Podesta, M., Jones, P. D., and Parker, D. E.: HadISDH: an updateable land surface specific humidity product for climate monitoring, Clim. Past, 9, 657–677, doi:10.5194/cp-9-657-2013, 2013. 84, 89

Winter, T. C., Rosenberry, D. O., and Sturrock, A. M.: Evaluation of 11 equations for determining evaporation for a small lake in the north central United States, Water Resour. Res., 31, 983–993, 1995. 100, 105

Wisser, D., Frolking, S., Douglas, E. M., Fekete, B. M., Vörösmarty, C. J., and Schumann, A. H.: Global irrigation water demand: Variability and uncertainties arising from agricultural and climate data sets, Geophys. Res. Lett., 35, L24408, doi:10.1029/2008GL035296, 2008. 83

ESDD
6, 81–132, 2015

Table 1. Bias-corrected meteorological data used in this study. The data sets were distributed by the ISI-MIP, after bias correction by the method proposed by Hempel et al. (2013).

Element	Bias correction
average temperature	additive
total precipitation	multiplicative
snowfall	multiplicative
shortwave radiation	multiplicative
longwave radiation	multiplicative
near-surface wind speed	multiplicative
surface pressure	multiplicative
relative humidity	uncorrected

ESDD
6, 81–132, 2015

Table 2. Global average of monthly SD [% RH] in relative humidity, shown in Fig. 4, for each land use.

GCMs	Mosaic 0	Mosaic 1	Mosaic 2	Mosaic 3
GFDL-ESM2M	20.3	26.2	23.9	17.6
HadGEM2-ES	11.7	24.3	20.1	13.4
IPSL-CM5A-LR	15.0	34.8	27.0	13.6
MIROC-ESM-CHEM	20.4	18.0	20.0	17.4
NorESM1-M	17.9	20.4	18.8	13.4

ESDD
6, 81–132, 2015

Table 3a. Results of the present (1971–2000) estimation and future (2070–2099) projection of irrigational water demand (IWD). The values in brackets are changes [%] relative to the present values. The range (the difference between the maximum and minimum) of the five GCMs is given in the bottom line.

GCMs	Global sum of IWD [$km^3\ yr^{-1}$] and relative change [%] Mosaic 0								
	present (1971–2000)	future (2070–2099) RCP2.6		RCP4.0		RCP6.0		RCP8.5	
GFDL-ESM2M	3254.6	3536.1	(+8.65)	3520.8	(+8.18)	3683.6	(+13.18)	3888.4	(+19.48)
HadGEM2-ES	3183.8	3154.5	(−0.92)	3369.1	(+5.82)	3279.2	(+3.00)	3495.3	(+9.78)
IPSL-CM5A-LR	3554.9	3695.5	(+3.96)	3737.2	(+5.13)	3943.7	(+10.94)	4222.0	(+18.77)
MIROC-ESM-CHEM	2809.0	3097.1	(+10.25)	3042.6	(+8.31)	3428.6	(+22.06)	3355.9	(+19.47)
NorESM1-M	2845.4	2918.8	(+2.58)	2978.5	(+4.68)	3055.6	(+7.38)	3250.2	(+14.22)
Ensemble mean	3129.5	3280.4	(+4.82)	3329.6	(+6.39)	3478.1	(+11.14)	3642.4	(+16.39)
Range	745.9	776.7		758.7		888.1		971.8	

ESDD
6, 81–132, 2015

Table 3b. Results of the present (1971–2000) estimation and future (2070–2099) projection of irrigational water abstraction from rivers (IWAR). The values in brackets are changes [%] relative to the present values. The range (the difference between the maximum and minimum) of the five GCMs is given in the bottom line.

GCMs	Global sum of IWAR [$km^3\ yr^{-1}$] and relative change [%] Mosaic 0 present (1971–2000)	future (2070–2099) RCP2.6		RCP4.0		RCP6.0		RCP8.5	
GFDL-ESM2M	1270.5	1281.9	(+0.90)	1286.5	(+1.26)	1291.6	(+1.66)	1326.2	(+4.39)
HadGEM2-ES	1278.4	1263.3	(−1.18)	1287.1	(+0.68)	1273.4	(−0.39)	1314.7	(+2.84)
IPSL-CM5A-LR	1341.3	1330.6	(−0.79)	1332.4	(−0.66)	1323.4	(−1.33)	1354.7	(+1.00)
MIROC-ESM-CHEM	1237.0	1250.6	(+1.09)	1238.6	(+0.12)	1269.9	(+2.66)	1234.8	(−0.18)
NorESM1-M	1217.7	1229.0	(+0.93)	1233.7	(+1.32)	1246.5	(+2.36)	1262.7	(+3.70)
Ensemble mean	1269.0	1271.1	(+0.17)	1275.7	(+0.53)	1281.0	(+0.95)	1298.6	(+2.33)
Range	123.6	101.6		98.7		76.9		119.9	

ESDD
6, 81–132, 2015

Table 4a. Results of the reference and sensitivity experiments with artificial biases of ±5 % RH – irrigational water demand (IWD). The values in brackets are changes [%] relative to the original values.

GCMs	Global sum of IWD [$km^3\,yr^{-1}$] and relative change [%]				
		Mosaic 0			
	original (1971–2000)	−5 % RH (1971–2000)		+5 % RH (1971–2000)	
GFDL-ESM2M	3254.6	3469.7	(+6.61)	3046.5	(−6.39)
HadGEM2-ES	3183.8	3410.7	(+7.13)	2964.0	(−6.90)
IPSL-CM5A-LR	3554.9	3786.7	(+6.52)	3329.8	(−6.33)
MIROC-ESM-CHEM	2809.0	3020.7	(+7.54)	2605.0	(−7.27)
NorESM1-M	2845.4	3048.0	(+7.12)	2649.7	(−6.88)

ESDD
6, 81–132, 2015

Table 4b. Results of the reference and sensitivity experiments with artificial biases of ±5 % RH – irrigational water abstraction from rivers (IWAR). The values in brackets are changes [%] relative to the original values.

GCMs	Global sum of IWAR [$km^3 yr^{-1}$] and relative change [%]				
		Mosaic 0			
	original (1971–2000)	−5 % RH (1971–2000)		+5 % RH (1971–2000)	
GFDL-ESM2M	1270.5	1318.9	(+3.81)	1221.2	(−3.88)
HadGEM2-ES	1278.4	1335.1	(+4.44)	1220.0	(−4.56)
IPSL-CM5A-LR	1341.3	1388.2	(+3.50)	1292.8	(−3.62)
MIROC-ESM-CHEM	1237.0	1292.0	(+4.45)	1180.2	(−4.60)
NorESM1-M	1217.7	1271.6	(+4.43)	1162.9	(−4.50)

ESDD
6, 81–132, 2015

Table 5. Global sum of irrigational water demand (IWD) and irrigational water abstraction from rivers (IWAR) [$km^3 yr^{-1}$] with bias-corrected humidity data. See Table 3a and b for comparison with uncorrected humidity data. The values in brackets are changes [%] relative to present values. The range (the difference between the maximum and minimum) of the five GCMs is given in the bottom line.

GCMs	IWD [$km^3 yr^{-1}$]			IWAR [$km^3 yr^{-1}$]		
	present 1971–2000	RCP 8.5 2070–2099		present 1971–2000	RCP 8.5 2070–2099	
GFDL-ESM2M	3132.1	3737.3	(+19.32)	1278.2	1338.4	(+4.71)
HadGEM2-ES	3225.9	3568.7	(+10.63)	1320.0	1338.4	(+1.39)
IPSL-CM5A-LR	3132.9	3729.2	(+19.03)	1259.5	1278.8	(+1.53)
MIROC-ESM-CHEM	2902.5	3455.8	(+19.06)	1263.3	1260.8	(−0.20)
NorESM1-M	2799.8	3193.3	(+14.05)	1221.4	1265.1	(+3.58)
Ensemble mean	3038.6	3536.9	(+16.40)	1268.5	1296.3	(+2.19)
Range	426.1	544.0		98.6	77.6	

ESDD
6, 81–132, 2015

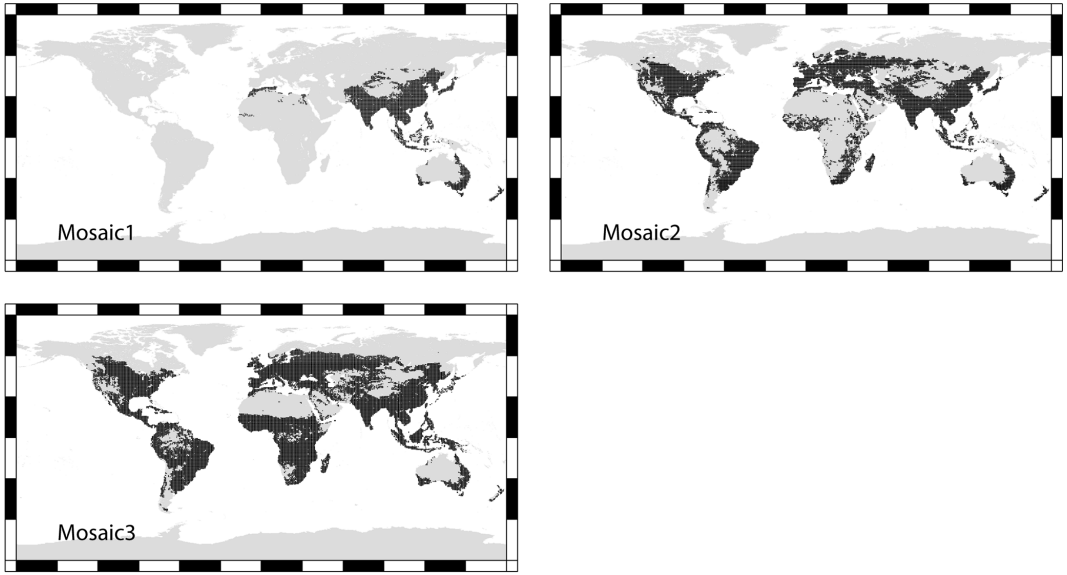

Figure 1. Geographical distribution of irrigated croplands – **(a)** double-cropping each year (Mosaic 1), **(b)** single-cropping each year (Mosaic 2) and **(c)** rain-fed cropland (Mosaic 3) – used in this study. The distributions are indicated in black.

ESDD
6, 81–132, 2015

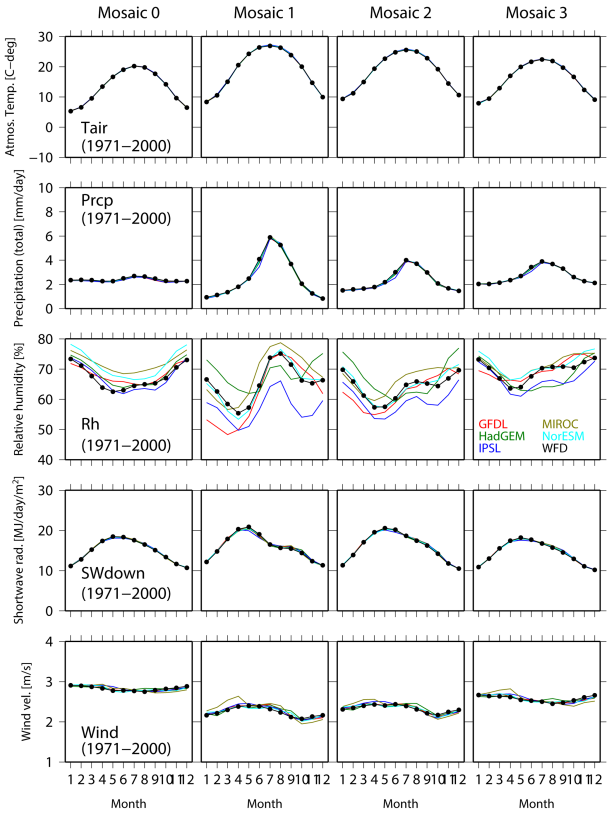

Figure 2. Monthly profiles of meteorological elements used in this study for 1971–2000. The results are aggregated over each type of land use, identified by the mosaic number. Profiles of the five GCMs are indicated in different colors: (red) GFDL, (green) HadGEM, (blue) IPSL, (dark yellow) MIROC and (light blue) NorESM. Profiles of the WATCH data are shown as black lines with dots.

ESDD
6, 81–132, 2015

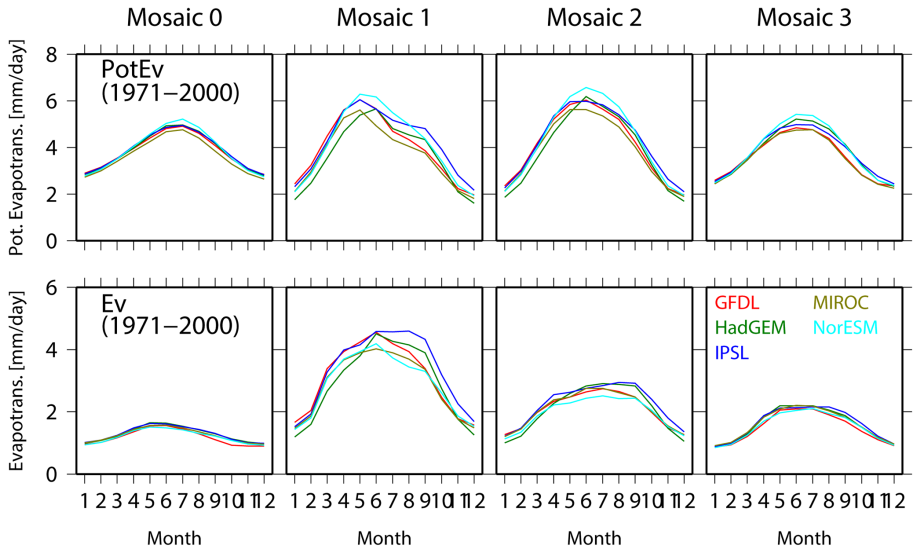

Figure 3. Monthly profiles of the potential evapotranspiration and evapotranspiration for 1971–2000 calculated in this study. The results are aggregated over the same land use. Profiles of the five GCMs are indicated in different colors: (red) GFDL, (green) HadGEM, (blue) IPSL, (dark yellow) MIROC and (light blue) NorESM.

ESDD
6, 81–132, 2015

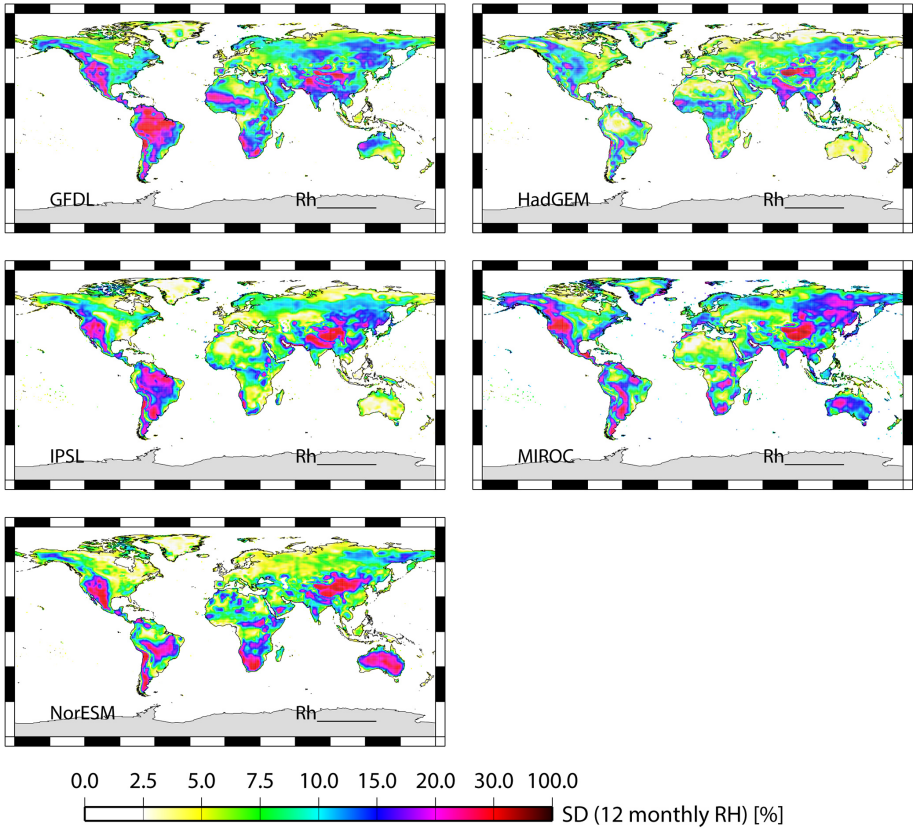

Figure 4. Geographical distribution of the SD from the WATCH data for the relative humidity. The SD was evaluated from 12 month climatological (1971–2000) data for each land cell.

ESDD
6, 81–132, 2015

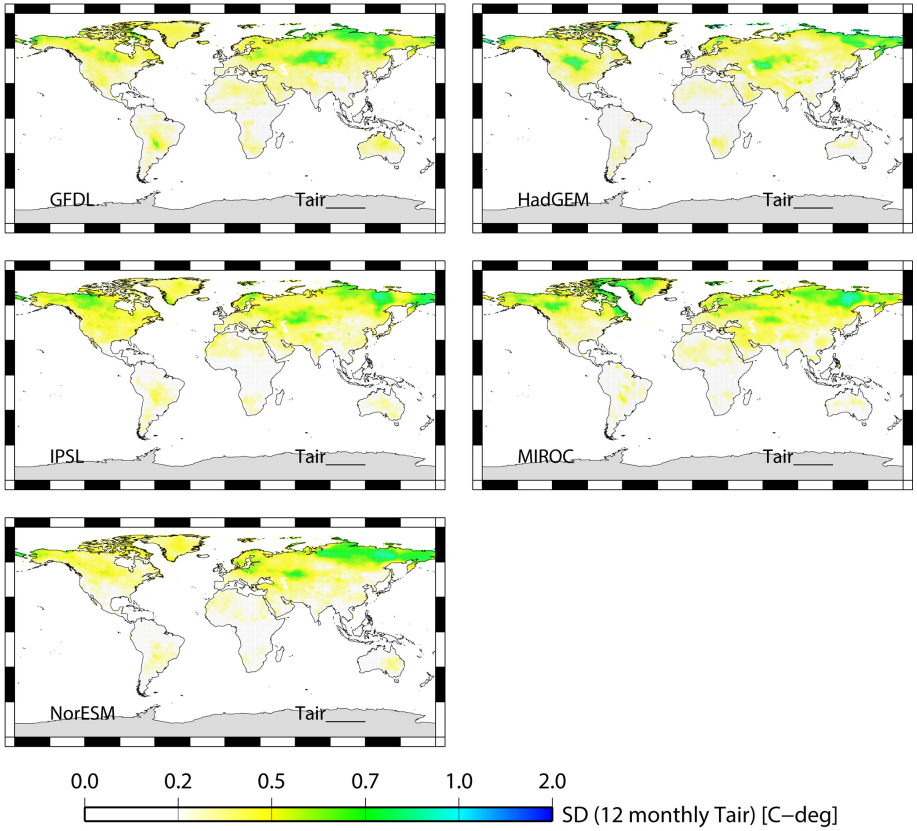

Figure 5. Same as Fig. 4 for the atmospheric temperature.

ESDD
6, 81–132, 2015

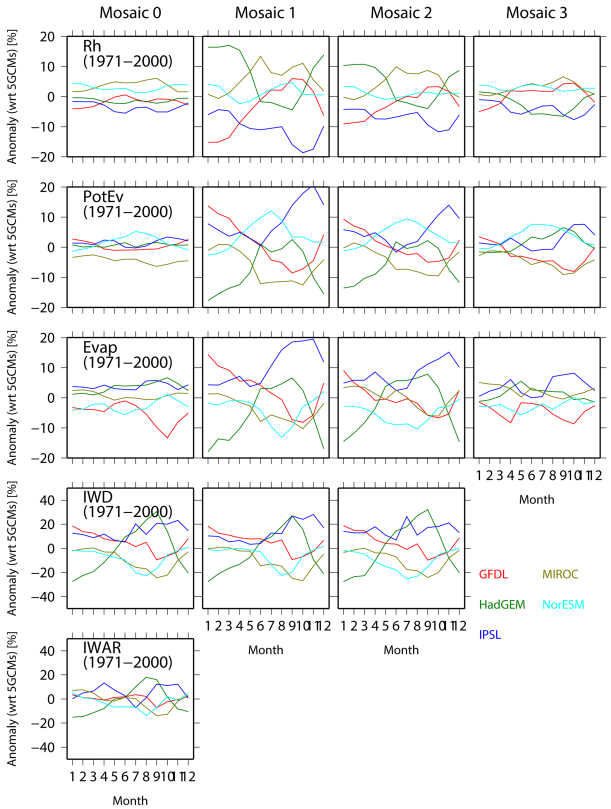

Figure 6. Monthly anomalies with respect to the ensemble mean of five GCMs for 1971–2000. The results are aggregated over each land use. The anomaly in each GCM is indicated in different colors: (red) GFDL, (green) HadGEM, (blue) IPSL, (dark yellow) MIROC and (light blue) NorESM. The panels from top to bottom show the relative humidity, potential evapotranspiration, evapotranspiration, irrigational water demand (IWD) and irrigational water abstraction from rivers (IWAR).

ESDD
6, 81–132, 2015

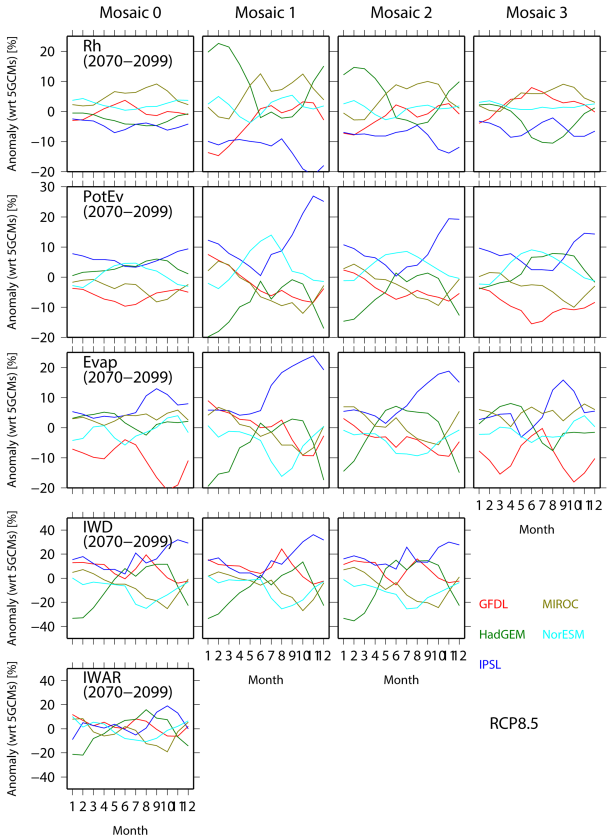

Figure 7. Same as in Fig. 6 but for the future period (2070–2099) under RCP 8.5.

ESDD
6, 81–132, 2015

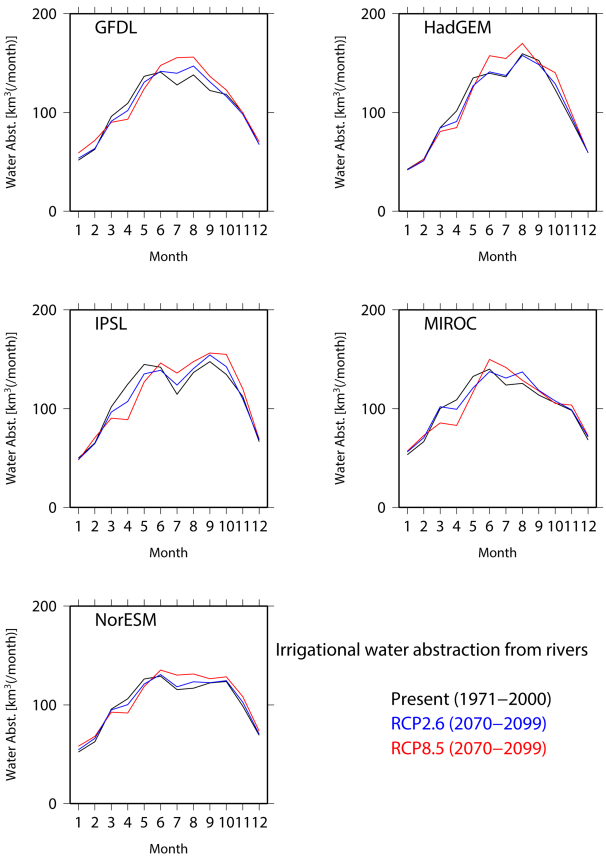

Figure 8. Monthly profiles of the global sum of present and future irrigational water abstraction from rivers (IWAR). Black, blue and red lines show the results of the present (1971–2000) estimation and future (2070–2099) projections under RCPs 2.6 and 8.5, respectively.

ESDD
6, 81–132, 2015

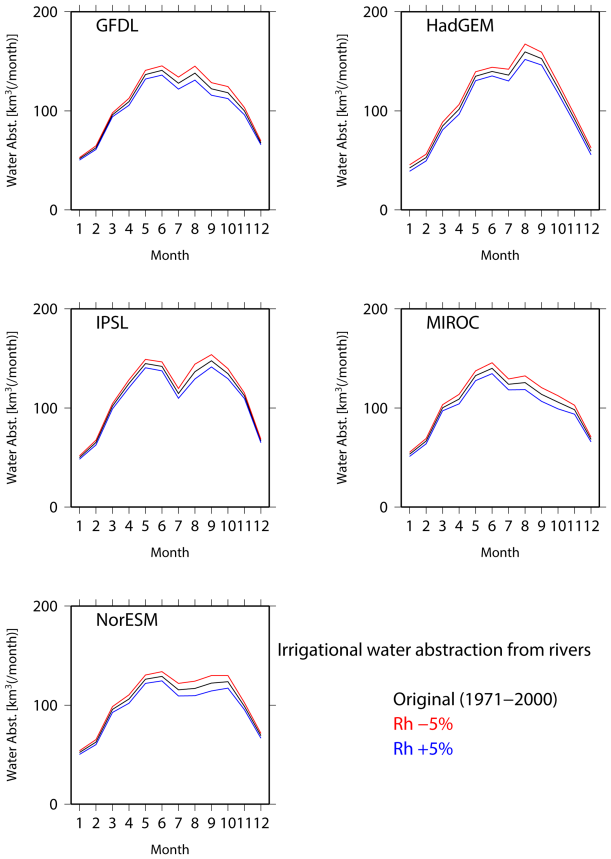

Figure 9. Monthly profiles of the global sum of irrigational water abstraction from rivers (IWAR) for the reference and sensitivity experiments with artificial biases of ±5 % RH. The analysis period is 1971–2000.

ESDD
6, 81–132, 2015

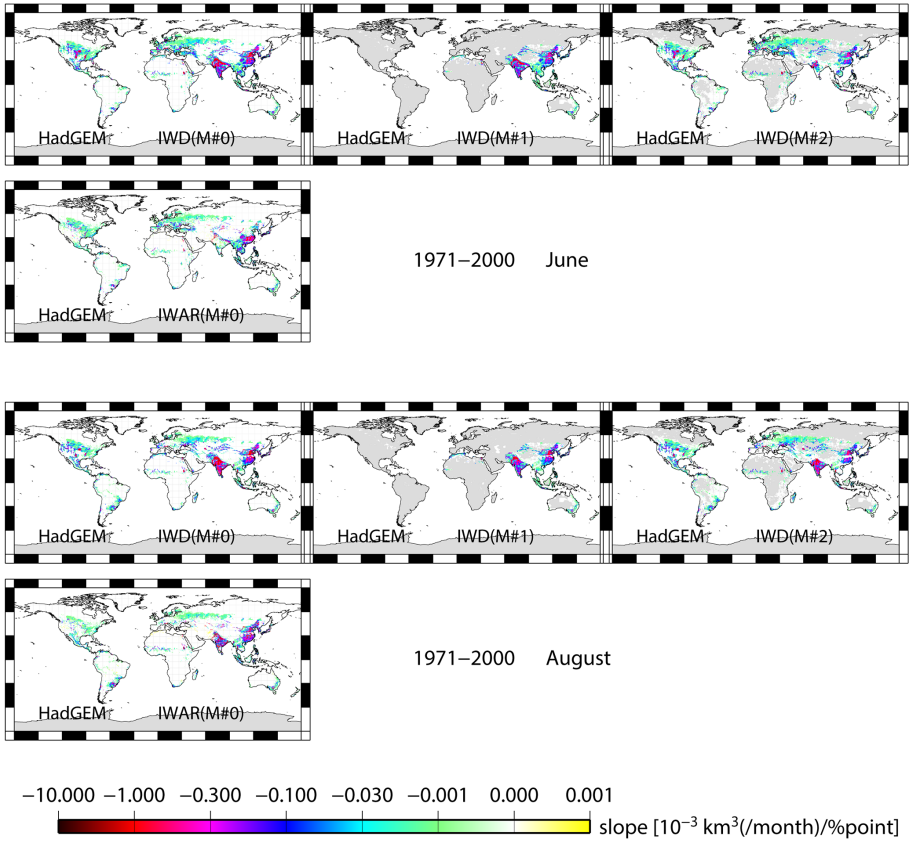

Figure 10. Geographical distribution of sensitivity, given by change in IWD or IWAR per change of 1 % RH in the relative humidity. HadGEM results for June and August are shown.

ESDD
6, 81–132, 2015

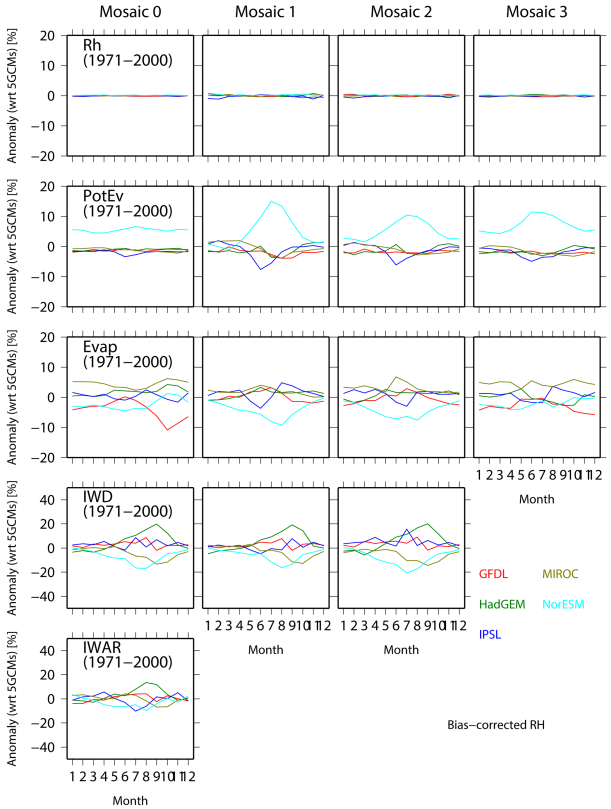

Figure 11. Monthly anomalies with respect to the ensemble mean in five GCMs with bias-corrected humidity data for 1971–2000. The results are aggregated over each land use. The anomaly in each GCM is indicated in different colors: (red) GFDL, (green) HadGEM, (blue) IPSL, (dark yellow) MIROC and (light blue) NorESM. The panels from top to bottom show the relative humidity, potential evapotranspiration, evapotranspiration, irrigational water demand (IWD) and irrigational water abstraction from rivers (IWAR).

ESDD
6, 81–132, 2015

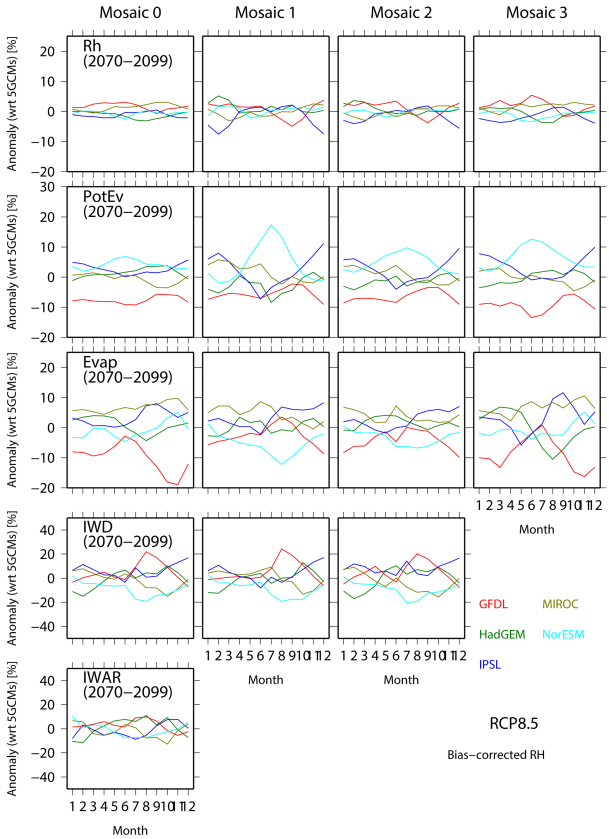

Figure 12. Same as in Fig. 11 but for the future period (2070–2099) under RCP 8.5.

ESDD
6, 81–132, 2015

Propagation of biases in humidity in the estimation of global irrigational water

Y. Masaki et al.

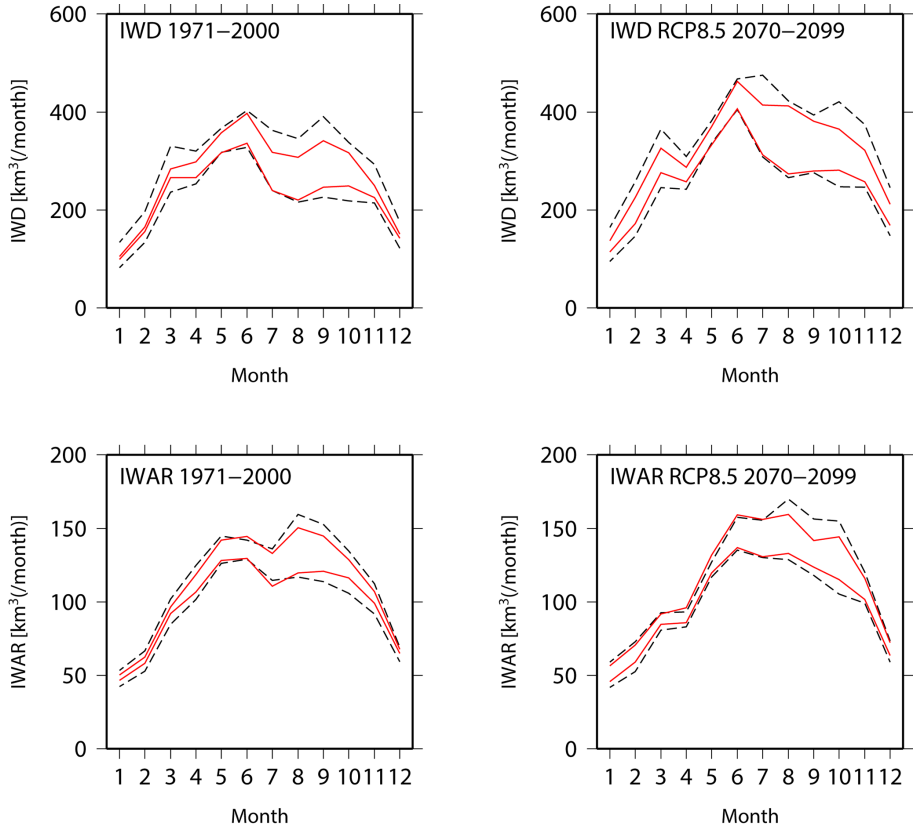

Figure 13. Changes in monthly ranges of irrigational water demand (IWD) and irrigational water abstraction from rivers (IWAR) after correcting humidity bias. Broken black and solid red lines show the results with uncorrected and bias-corrected humidity data, respectively. Each pair of lines gives the maximum and minimum values for the five GCMs.

ESDD
6, 81–132, 2015